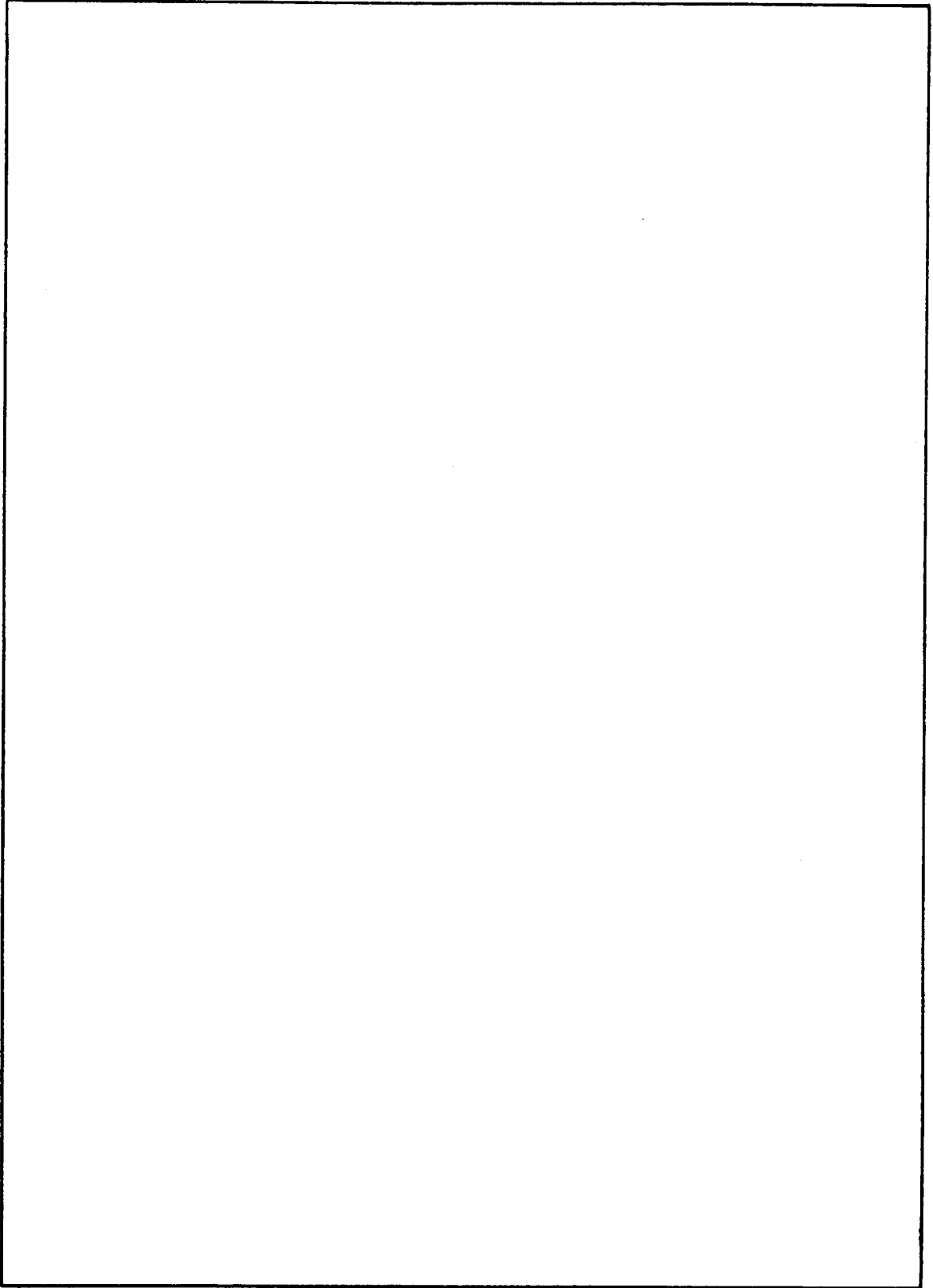


REPORT DOCUMENTATION PAGE		READ INSTRUCTIONS BEFORE COMPLETING FORM
1. REPORT NUMBER NRL Report 8114	2. GOVT ACCESSION NO.	3. RECIPIENT'S CATALOG NUMBER
4. TITLE (and Subtitle) ANGLE MEASUREMENTS FOR BROAD-BEAM-ARRAY RADARS		5. TYPE OF REPORT & PERIOD COVERED Interim report on one phase of a continuing NRL Problem
		6. PERFORMING ORG. REPORT NUMBER
7. AUTHOR(s) Ben H. Cantrell		8. CONTRACT OR GRANT NUMBER(s)
9. PERFORMING ORGANIZATION NAME AND ADDRESS Naval Research Laboratory Washington, D.C. 20375		10. PROGRAM ELEMENT, PROJECT, TASK AREA & WORK UNIT NUMBERS NRL Problem R02-54 Project ZF 12-151-001, 62712N
11. CONTROLLING OFFICE NAME AND ADDRESS Department of the Navy Office of Naval Research Arlington, Va. 22217		12. REPORT DATE May 23, 1977
		13. NUMBER OF PAGES 26
14. MONITORING AGENCY NAME & ADDRESS (if different from Controlling Office)		15. SECURITY CLASS. (of this report) Unclassified
		15a. DECLASSIFICATION/DOWNGRADING SCHEDULE
16. DISTRIBUTION STATEMENT (of this Report) Approved for public release; distribution unlimited.		
17. DISTRIBUTION STATEMENT (of the abstract entered in Block 20, if different from Report)		
18. SUPPLEMENTARY NOTES		
19. KEY WORDS (Continue on reverse side if necessary and identify by block number) Search radars Angle measures		
20. ABSTRACT (Continue on reverse side if necessary and identify by block number) This report describes the problems in measuring the angle of a target with broadbeam radars. It is shown that if the array is cross-level stabilized, reasonably good azimuth measurements can be made and the elevation measures are good except for about 7 to 8 degrees down to the horizon. For the situation with no cross-level stabilization present, two solution techniques were suggested.		



CONTENTS

INTRODUCTION	1
REVIEW OF PERTINENT TOPICS	1
Antenna Patterns	1
Multipath Propagation	2
Errors Arising in Conventional Angle Measurements	5
Effects of Scanning Off Axis	7
Errors Due to Cone Correction	8
Array Drive Equations	10
STABLE-PLATFORM RADAR ANGLE MEASUREMENTS	14
UNSTABLE-PLATFORM RADAR ANGLE MEASUREMENTS ..	16
SUMMARY	18
REFERENCES	19
APPENDIX A – Complex Models	20
APPENDIX B – Error Propagation Through Transformations ..	22

ANGLE MEASUREMENTS FOR BROAD-BEAM-ARRAY RADARS

INTRODUCTION

Broad-beam-array radars will be considered in this report. Because of the frequency (less than 1 GHz) and antenna-size limitation on the ship, fairly broad beams are anticipated. This naturally raises the question as to the accuracy with which the angle measures of the target can be made, a topic which is the concern of this report. It is not the purpose here to describe the entire radar. The antenna would be an array with beamwidths of 5° and 15° in azimuth and elevation respectively. Four arrays would be required to cover the full 360° in azimuth. The topics affecting the angle measurements will be briefly reviewed. These include antenna patterns, multipath propagation, noise, scanning the array off axis, and the roll and pitch of the ship. A design and rough results will then be given for the case of the radar being stabilized with respect to ship motion. Finally a means will be formulated for obtaining azimuth and elevation measurements when both sea-reflected multipath propagation and ship motion are present.

REVIEW OF PERTINENT TOPICS

Antenna Patterns

The Kirchhoff-Fresnel theory can be used to determine the antenna patterns for a planer-array antenna. A simplified form of it in the far field is

$$E = \frac{je^{-j2\pi R/\lambda}}{2\lambda R} (1 + \cos \theta) \iint A(x,y) e^{j[(\alpha x/d) + (\epsilon y/h)]} dx dy, \quad (1)$$

where

E = electric field,

R = range,

λ = wavelength,

θ_n = angle between the line normal to the array and the line in a plane normal to the array connecting the field point to the array (Fig. 1),

$A(x,y)$ = power distribution across the array,

d = aperture width,

h = aperture height,

$$\alpha = \frac{2\pi d}{\lambda} \cos \theta \tan az \simeq \frac{2\pi d}{\lambda} az, \quad (2)$$

and

$$\epsilon = \frac{2\pi h}{\lambda} \cos \theta \tan el \simeq \frac{2\pi h}{\lambda} el, \quad (3)$$

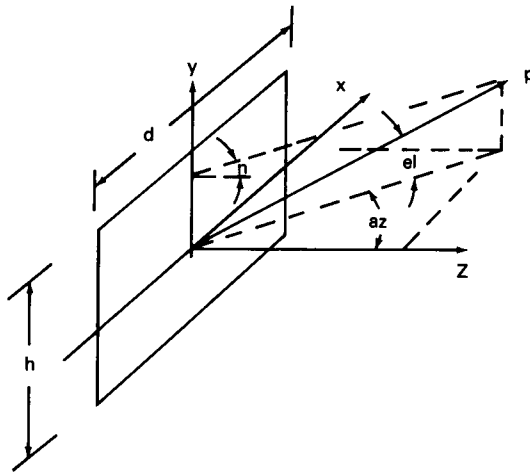


Fig. 1 - Antenna geometry

with az and el being the azimuth and elevation angles. The variation in θ is neglected, and the aperture field is assumed to be factorable, so that

$$E = \text{const } f(\epsilon)f(\alpha), \quad (4)$$

where

$$f(\epsilon) = \int_{-h/2}^{h/2} A(y)e^{+j\epsilon y/h} dy$$

and

$$f(\alpha) = \int_{-d/2}^{d/2} A(x)e^{+j\alpha x/d} dx.$$

The antenna patterns then is assumed to be

$$G(az, el) = G(az)G(el) = f(\epsilon)f(\alpha). \quad (5)$$

The set of antenna patterns which will be used is shown in Table 1. These are for 0° pointing angles. Pointing angles other than normal to the array face will be considered later. The cosine-squared and double-angle-sine patterns are typical of the sum and difference patterns in a monopulse radar. The double-null pattern is an even function with a null at zero.

Multipath Propagation

A simple geometrical optics model is used to describe the sea-reflected multipath propagation. The geometry is shown in Fig. 2. The radiation from the antenna to the target and the backscatter will be propagated by the direct path and the reflected path. At each point on the antenna aperture the signal strength is the sum of the direct signal and the indirect signal, whose relative phase varies. The resultant returned signal is obtained by summing the signals across the aperture. The results of this simple model are well known [1] and are

$$S = A [G(el)e^{+j2\pi h_a el/\lambda} + \rho G(-el)e^{-j(2\pi h_a el/\lambda + \phi)}], \quad (6)$$

Table 1 — Antenna Patterns

Name	$A(x)$	$f(\alpha)$
Cosine squared	$\cos^2 \frac{\pi x}{d}$	$\frac{\frac{d\pi}{2} \sin \frac{\alpha}{2}}{\pi^2 - \left(\frac{\alpha}{2}\right)^2}$
Double-angle sine	$\sin \frac{2\pi x}{d}$	$\frac{d\pi \sin \frac{\alpha}{2}}{\pi^2 - \left(\frac{\alpha}{2}\right)^2}$
Double null	$\cos \frac{2\pi x}{d}$	$\frac{d^2 \left(\frac{\alpha}{2}\right) \sin \frac{\alpha}{2}}{\pi^2 - \left(\frac{\alpha}{2}\right)^2}$

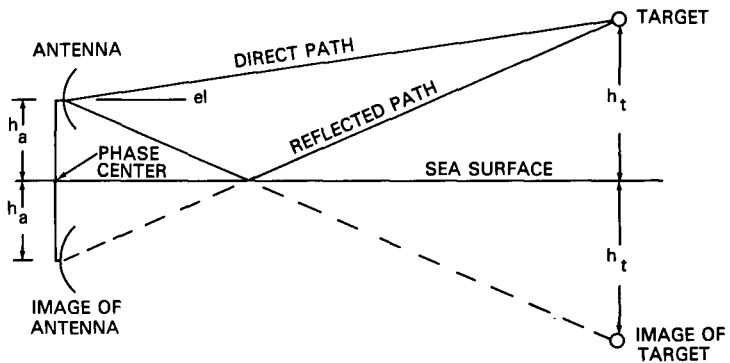


Fig. 2 — Multipath-propagation geometry

where S is the returned signal, A is the amplitude, h_a is the antenna height, el is the elevation angle, ρ is the reflection coefficient, and ϕ is the phase shift at sea surface. For a smooth sea the reflection coefficients are

$$\rho_h e^{j\phi_h} = \frac{\sin el - \sqrt{\epsilon_c - \cos^2 el}}{\sin el + \sqrt{\epsilon_c - \cos^2 el}} \quad (7)$$

and

$$\rho_v e^{j\phi_v} = \frac{\epsilon_c \sin el - \sqrt{\epsilon_c - \cos^2 el}}{\epsilon_c \sin el + \sqrt{\epsilon_c - \cos^2 el}}, \quad (8)$$

where $\epsilon_c = \epsilon_1 - j60\lambda\sigma$ is the complex dielectric coefficient shown in Table 2 for various frequencies [2]. The model presented is fairly good as long as the Rayleigh criterion,

$$\Delta h < \frac{1}{8} \frac{\lambda}{\sin \epsilon l},$$

where Δh is the wave height, is met. For higher sea states the picture is more clouded. We will assume for the remainder of the report that for the higher sea states the reflection coefficient magnitude and phase shift are unknown and vary with time. A more detailed discussion is given in Appendix A. In addition the dominant reflection is near an angle equal to but opposite of the target elevation. If several dominant reflectors are present, terms would have to be added to (6) to account for them. Two plots of the radar signal level for zero sea states are given in Fig. 3. The ordinate value of 0 dB is for the free-space range at the peak of the antenna pattern. These are the usual lobing plots associated with a ship's radar coverage.

Table 2 — Dielectric and Conductivity Values Used in the Reflection-Coefficient Calculations

Frequencies (MHz)	Value of Dielectric Constant ϵ_1 (F/m)	Value of Conductivity σ (mhos/m)
$f < 1500$	80	4.3
1500 to 3000	$80 - 0.00733 (f - 1500)$	$4.3 + 0.00148 (f - 1500)$
3000 to 10,000	$69 - 0.00243 (f - 3000)$	$6.52 + 0.001314 (f - 3000)$

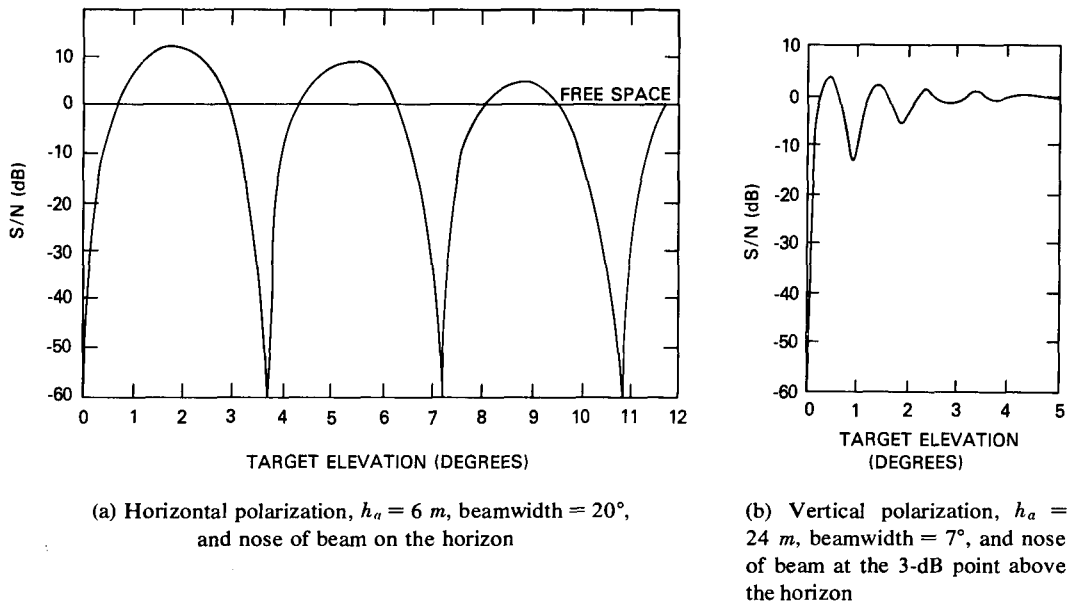


Fig. 3 — Lobing due to multipath propagation of radiation with $\lambda = 76$ cm over a smooth sea

Errors Arising in Conventional Angle Measurements

Two conventional means of obtaining angle measurements in free space are beamsplitting for scanning beams and the monopulse method for stationary beams. The scanning beam is of no concern here. The angle measurement by the monopulse method is illustrated by taking the ratio of the signals from the double-angle-sine pattern (difference pattern) and cosine-squared antenna pattern (sum pattern) given in Table 1. This yields

$$\mathcal{R}_\alpha = \frac{d\pi \sin \frac{\alpha}{2} / \left[\pi^2 - \left(\frac{\alpha}{2} \right)^2 \right]}{\frac{d}{2} \left[\left[\sin \frac{\alpha}{2} \right] / \frac{\alpha}{2} \right] \pi^2 / \left[\pi^2 - \left(\frac{\alpha}{2} \right)^2 \right]} \tag{9}$$

The azimuth angle can be found from (2) and (9) and is

$$az = (\lambda/2d)\mathcal{R}_\alpha, \tag{10}$$

and the elevation angle can be found from (3) and an equation similar to (9):

$$el = (\lambda/2h)\mathcal{R}_\epsilon. \tag{11}$$

Since the beamwidth is θ_{BW} equals 2.88 $(\lambda/2d)$ or equals 2.88 $(\lambda/2h)$,

$$az = \mathcal{R}_\alpha (\theta_{BW}/2.88) \tag{12}$$

and

$$el = \mathcal{R}_\epsilon (\theta_{BW}/2.88). \tag{13}$$

The azimuth, or elevation, is directly proportional to the ratio of the difference signal to the sum signal.

The effect of noise on the monopulse measurement [3] is given in Fig. 4. At a 13-dB signal-to-noise ratio S/N the monopulse error (standard deviation) is 0.1 beamwidth. For a rough approximation the slope of the monopulse curve, given by (12) or (13), is 0.4 beamwidth. Therefore the error could be computed by multiplying the slope of the monopulse curve by $0.1/0.4 = 0.25$. For any other monopulse curve (or any other curve) formed by the ratios found in this report the angle error would be estimated by multiplying the slope of the curve by 0.25.

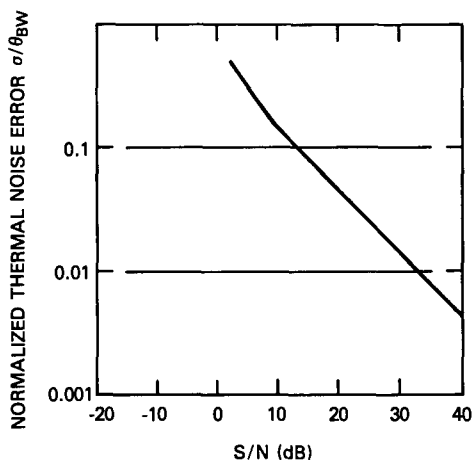


Fig. 4 – Effect of noise on the monopulse measurement error normalized to a beamwidth

Angle measurements in sea-reflected multipath propagation are considered next. In Fig. 5a the 3-dB contour of a pencil-beam radar is shown centered on the horizon for the case when the beam has no cross-level error. When no cross-level error is present, the target and its image lie at the same azimuth but at different elevations with respect to their defining planes. When cross-level error is present, the target and images are at different angles in both the azimuth and elevation planes. A well-established fact in radar is that multiple unresolved targets can cause large angle errors. To simplify the problem, it will be assumed the cross-level angle (Z in Fig. 5b) is zero and therefore azimuth and elevation measurements can be made independently. In a later section nonzero cross-level angles will be considered.

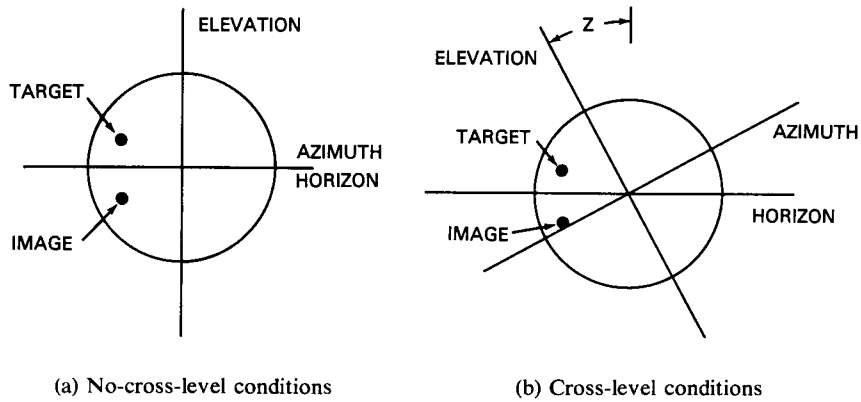


Fig. 5 – Target and image positions within the 3-dB contour of the beam of a pencil-beam radar

One means of measuring the elevation angle when there is sea-reflected multipath propagation was suggested by White [4]. For two antenna patterns G_A and G_B the returned signal voltages in the form of (6), with $\phi = 180^\circ$, for horizontal polarization are

$$V_A = A [G_A(\text{el})e^{+j\theta} - \rho G_A(-\text{el})e^{-j\theta}] \quad (14)$$

and

$$V_B = A [G_B(\text{el})e^{+j\theta} - \rho G_B(-\text{el})e^{-j\theta}]. \quad (15)$$

Taking the ratio \mathcal{R} of the two voltages yields

$$\mathcal{R} = \frac{V_B}{V_A} = \frac{G_B(\text{el})}{G_A(\text{el})} \frac{e^{+j\theta} - \rho e^{-j\theta} \frac{G_B(-\text{el})}{G_B(\text{el})}}{e^{+j\theta} - \rho e^{-j\theta} \frac{G_A(-\text{el})}{G_A(\text{el})}}. \quad (16)$$

By requiring symmetry of the two beams with respect to the horizon, which means that

$$G_B(-\text{el})/G_B(\text{el}) = G_A(-\text{el})/G_A(\text{el}), \quad (17)$$

the multipath terms in (16) cancel out, leaving the ratio of the two antenna patterns: $G_B(\text{el})/G_A(\text{el})$. Then the ratio can be solved for the elevation angle. When even-function antenna patterns about the horizon are used, multipath terms can be canceled in the ratio. As an

example using the double-null pattern for $G_B(\text{el})$ and the cosine-squared pattern for $G_A(\text{el})$, which are defined in Table 1, the ratio becomes

$$\mathcal{R} = \frac{2d \frac{\alpha}{2} \sin \frac{\alpha}{2} / \left[\pi^2 - \left(\frac{\alpha}{2} \right)^2 \right]}{\frac{d}{2} \left[\left(\sin \frac{\alpha}{2} \right) / \frac{\alpha}{2} \right] \pi^2 / \left[\pi^2 - \left(\frac{\alpha}{2} \right)^2 \right]} = \alpha^2 / \pi^2. \quad (18)$$

Using (2) and (18) the elevation angle becomes

$$\text{el} = \frac{\lambda}{2d} \sqrt{\mathcal{R}}. \quad (19)$$

For ratios near zero the slope (sensitivity) is small and the ability to measure elevation in the presence of noise is poor. In addition the received power has many deep nulls as a function of elevation for reflection coefficients near unity because of the symmetry about the horizon in the example used. Improved antenna patterns using this technique will be considered later.

Effects of Scanning Off Axis

When an array is scanned off axis, two effects must be considered. First the effective aperture width d_e decreases by

$$d_e = d \cos \text{az}. \quad (20)$$

The second effect is that the peak of the beam steers in both the elevation and azimuth along cones. This is illustrated in Fig. 6, which shows the cone for the azimuth case. The array is in the yz plane normal to the x axis. The azimuth az and elevation el represent the target's position. The array steering angles are γ and δ . The cone shown in Fig. 6 is defined as follows. The phase is the same at the array for any target along a cone defined by rotating a line from the array to a target about the y axis such that the angle between the line and the y axis is always $90^\circ - \gamma$. The other cone of constant phase is defined by rotating from the array to the target about the z axis, where the angle between the line and the z axis is $90^\circ - \delta$. The relations between the beam pointing angles and the beam steering angles are [5]

$$\delta = \text{el} \quad (21)$$

and

$$\sin \gamma = \cos \text{el} \sin \text{az}. \quad (22)$$

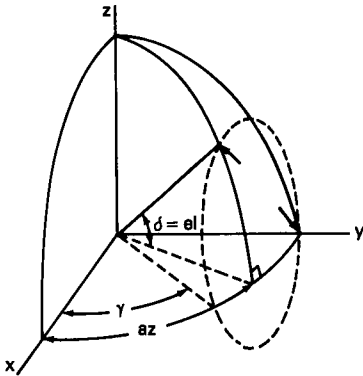


Fig. 6 - Relationship of beam pointing angles az and el to beam steering angles γ and δ

These results are shown graphically in Fig. 7. The results show that the azimuth γ measured by the radar is coupled to the true azimuth by (22). To find the true target azimuth, the elevation must be known.

The antenna patterns are then written as

$$G(\gamma, el) = G(\gamma - \gamma_0) G(el - el_0), \quad (23)$$

where $G(\gamma - \gamma_0)$ might be the cosine-squared antenna pattern

$$G(\gamma - \gamma_0) = \frac{d}{2} \frac{\sin [(\pi d_e/\lambda) (\gamma - \gamma_0)]}{(\pi d_e/\lambda) (\gamma - \gamma_0)} \frac{\pi^2}{\pi^2 - [(\pi d_e/\lambda) (\gamma - \gamma_0)]^2}, \quad (24)$$

where d_e is the effective aperture, γ_0 is the angle steered off in azimuth, and, by (22),

$$\gamma = \sin^{-1}(\cos el \sin az).$$

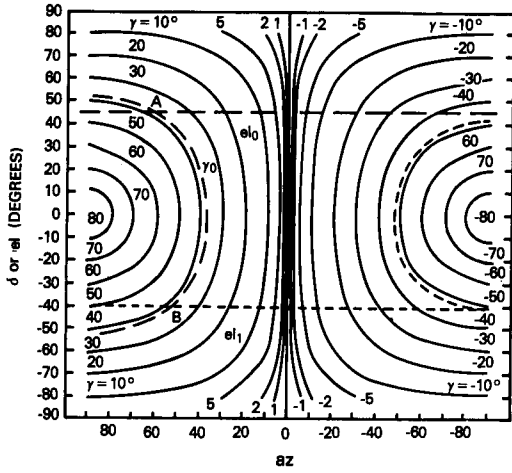


Fig. 7 - Beam pointing angles az and el in relation to beam steering angles γ and δ for a hemispheric volume

Errors Due To Cone Correction

Errors in measuring the steered elevation δ and γ result in errors in the true azimuth az . Since (22) is approximately linear in a region, these errors can be studied by using a truncated Taylor series expansion

$$az = az_0 + C_{11} \Delta \gamma + C_{22} \Delta \delta \quad (25)$$

where

$$C_{11} = \frac{\partial az}{\partial \gamma} = \cos \gamma / \sqrt{\cos^2 \delta - \sin^2 \gamma} \quad (26)$$

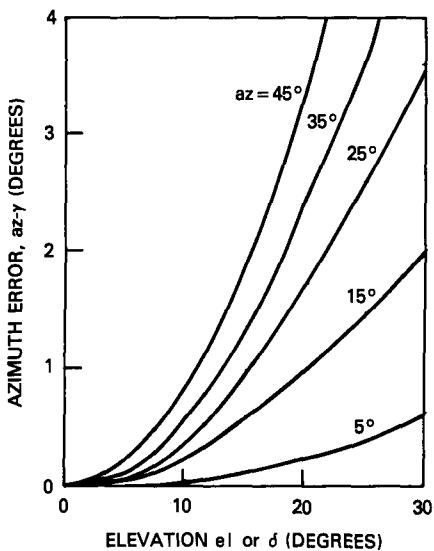
and

$$C_{22} = \frac{\partial az}{\partial \delta} = \sin \gamma \tan \delta / \sqrt{\cos^2 \delta - \sin^2 \gamma}. \quad (27)$$

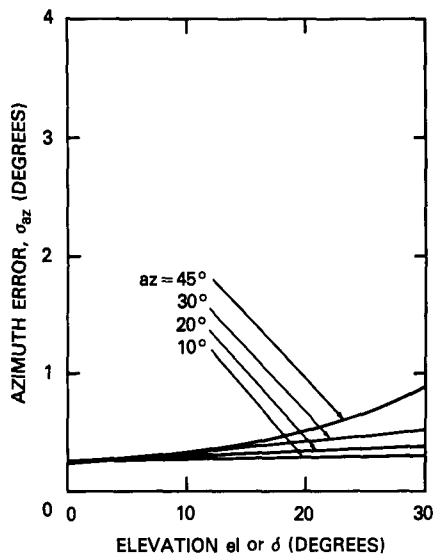
The standard deviation in estimating the azimuth is then

$$\sigma_{az} = \sqrt{C_{11}^2 \sigma_\gamma^2 + C_{22}^2 \sigma_\delta^2}. \quad (28)$$

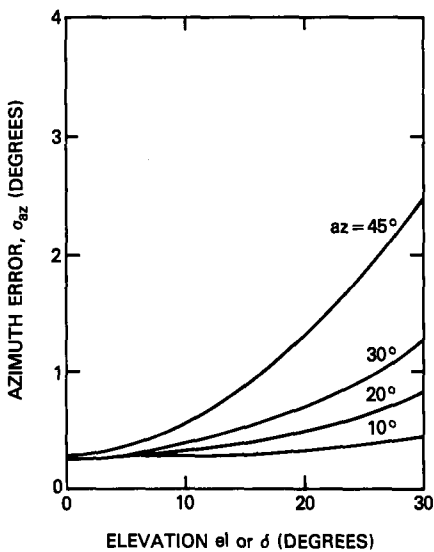
Figure 8a illustrates the error in azimuth if no elevation information is present. Figures 8b, 8c, and 8d illustrate typical errors in estimating azimuth for various amounts of elevation accuracy. Several things are interesting. At the low angles good elevation estimates are not necessary to correct the effects of the cone. However for large angles scanned off axis in both azimuth and elevation, elevation accuracies approaching 1° are required to make a good azimuth correction.



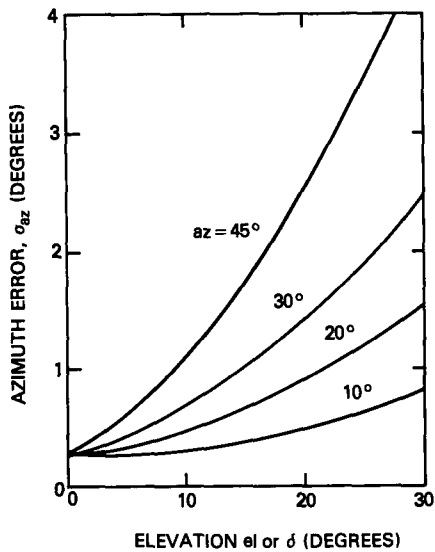
(a) No knowledge of elevation



(b) For $\sigma_\delta = 1^\circ$ and $\sigma_\gamma = 0.25^\circ$



(c) For $\sigma_\delta = 3^\circ$ and $\sigma_\gamma = 0.25^\circ$



(d) For $\sigma_\delta = 6^\circ$ and $\sigma_\gamma = 0.25^\circ$

Fig. 8 - Azimuth errors when scanning off axis

Array Drive Equations

All the discussion thus far, except for a brief comment earlier, has assumed that the array was on a stable platform. However the platforms of present-day shipboard radars are not stabilized. The equations required to drive the array are developed in this section.

The coordinate system in deck coordinates (x_d, y_d, z_d) is shown in Fig. 9. The Cartesian coordinates are related to the spherical coordinates by

$$x_d = r \cos e_d \sin a_d, \tag{29}$$

$$y_d = r \cos e_d \cos a_d, \tag{30}$$

and

$$z_d = r \sin e_d, \tag{31}$$

where the y_d axis lies along the deck of the ship in the aft-to-bow direction and the z_d axis is perpendicular to the deck of the ship. The gimbals of the gyro are set so that the roll axis is attached to the ship and the pitch axis is attached to the roll platform. The roll is positive when the deck is down on the port side and the pitch is positive when the bow is down.

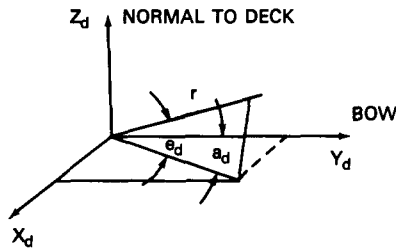


Fig. 9 - Deck coordinates

The relation between the stabilized coordinates and the deck coordinates is obtained through two rotations and is

$$\begin{bmatrix} x_s \\ y_s \\ z_s \end{bmatrix} = T \begin{bmatrix} x_d \\ y_d \\ z_d \end{bmatrix} \tag{32}$$

or

$$\begin{bmatrix} x_d \\ y_d \\ z_d \end{bmatrix} = T^t \begin{bmatrix} x_s \\ y_s \\ z_s \end{bmatrix}, \tag{33}$$

where T^t is the transpose of T :

$$T = \begin{bmatrix} \cos R & 0 & -\sin R \\ \sin R \sin P & \cos P & \cos R \sin P \\ \sin R \cos P & -\sin P & \cos R \cos P \end{bmatrix}, \tag{34}$$

in which R and P are the roll and pitch respectively. Sometimes these are placed into polar form by noting

$$\sin e_d = z_d/r \tag{35}$$

and

$$\tan az_d = x_d/y_d. \quad (36)$$

By combining (29) through (31) and (33) through (36), one obtains the standard stabilization equations

$$\tan az_d = \frac{\cos el_s \sin az_s \cos R + (\cos el_s \cos az_s \sin P + \sin el_s \cos P) \sin R}{\cos el_s \cos az_s \cos P - \sin el_s \sin P} \quad (37)$$

and

$$\begin{aligned} \sin el_d &= (\cos el_s \cos az_s \sin P + \sin el_s \cos P) \cos R \\ &\quad - \cos el_s \sin az_s \sin R. \end{aligned} \quad (38)$$

where the subscript *s* indicates the stabilized coordinates. Similarly the inverse relations can be found. The error propagation can be studied by using a Taylor series expansion. However the cases of interest are more complex than the standard stabilization equations. The effect of scanning the radar off axis can be incorporated into the equation, the orientation of the array on the ship must be accounted for, and, if any mechanical stabilization is used, the results must reflect this.

We begin by aligning the axis with the array face. From Fig. 9 the deck azimuth was measured clockwise from the y_d axis in the $x_d y_d$ plane. It is desirable to measure azimuth from the array face rather from the bow of the ship, assuming the antenna lies in the $x_d z_d$ plane. This is accomplished by rotating the deck coordinate through an angle \mathcal{A} about the z_d axis such that the y axis is normal to the array face. If in addition the array is tilted back by an angle \mathcal{B} , the coordinates must be rotated about the x axis until the xz plane lies on the plane of the array. The new face coordinate system (x_f, y_f, z_f) has the y_f axis normal to the array, and the array lies in the $x_f y_f$ plane. The relation between the coordinates is

$$\begin{bmatrix} x_d \\ y_d \\ z_d \end{bmatrix} = W \begin{bmatrix} x_f \\ y_f \\ z_f \end{bmatrix}, \quad (39)$$

where $W W^t = I$ and

$$W = \begin{bmatrix} \cos \mathcal{A} & \sin \mathcal{A} \cos \mathcal{B} & -\sin \mathcal{A} \sin \mathcal{B} \\ -\sin \mathcal{A} & \cos \mathcal{A} \cos \mathcal{B} & -\cos \mathcal{A} \sin \mathcal{B} \\ 0 & \sin \mathcal{B} & \cos \mathcal{B} \end{bmatrix}. \quad (40)$$

The stabilized coordinates and face coordinates are then related by

$$\begin{bmatrix} x_s \\ y_s \\ z_s \end{bmatrix} = TW \begin{bmatrix} x_f \\ y_f \\ z_f \end{bmatrix} \quad (41)$$

and

$$\begin{bmatrix} x_f \\ y_f \\ z_f \end{bmatrix} = W^t T^t \begin{bmatrix} x_s \\ y_s \\ z_s \end{bmatrix}. \quad (42)$$

The effects of the array pointing at the intersection of two cones is next incorporated. The angles γ and δ are defined by

$$\sin \gamma = \frac{x_f}{\sqrt{x_f^2 + y_f^2}} \quad (43)$$

and

$$\cos \delta = \sqrt{x_f^2 + y_f^2}/r. \quad (44)$$

From use of (22), (43), and (44) the beam steering angles in azimuth and elevation are

$$\gamma = \sin^{-1}(x_f/r) \quad (45)$$

and

$$\delta = \text{el}_d = \sin^{-1}(z_f/r). \quad (46)$$

If the previous transformations are used, the beam steering angles can be related to the beam's stabilized position by

$$\begin{aligned} \sin \gamma &= \cos \mathcal{A} \cos R \cos \text{el}_s \sin \text{az}_s \\ &+ (\cos \mathcal{A} \sin R \sin P - \sin \mathcal{A} \cos P) \cos \text{el}_s \cos \text{az}_s \\ &+ (\cos \mathcal{A} \sin R \cos P + \sin \mathcal{A} \sin P) \sin \text{el}_s \end{aligned} \quad (47)$$

and

$$\begin{aligned} \sin \delta &= (-\sin \mathcal{B} \sin \mathcal{A} \cos R - \sin R \cos \mathcal{B}) \cos \text{el}_s \sin \text{az}_s \\ &+ (-\sin \mathcal{B} \sin \mathcal{A} \sin R \sin P - \sin \mathcal{B} \cos \mathcal{A} \cos P \\ &+ \cos \mathcal{B} \cos R \sin P) (\cos \text{el}_s \cos \text{az}_s) \\ &+ (-\sin \mathcal{B} \sin \mathcal{A} \sin R \cos P + \sin \mathcal{B} \cos \mathcal{A} \sin P \\ &+ \cos \mathcal{B} \cos R \cos P) (\sin \text{el}_s), \end{aligned} \quad (48)$$

where \mathcal{A} and \mathcal{B} are the array orientation angles on the ship, R and P are the roll and pitch angles, az_s and el_s are the azimuth and elevation in stabilized coordinates, and γ and δ are the beam pointing angles.

Conversely, if a target's angular position is measured in the beam steering coordinates, the target's position in stabilized coordinates can be obtained with relations which are the inverse of (47) and (48). These are obtained by finding

$$\text{az}_s = \tan^{-1} x_s/y_s \quad (49)$$

and

$$\text{el}_s = \sin^{-1} z_s/r. \quad (50)$$

When the Cartesian coordinates are converted to polar coordinates at the array face, the cone effect must be included by noting

$$\sin \text{az}_f = \sin \gamma / \cos \delta \quad (51)$$

and

$$\cos \text{az}_f = \sqrt{(\cos^2 \delta - \sin^2 \gamma) / \cos \delta}. \quad (52)$$

This is incorporated into the required Cartesian-to-spherical-coordinate conversions:

$$x_f = r \cos e_f \sin a_f = r \sin \gamma, \quad (53)$$

$$y_f = r \cos e_f \sin a_f = r \sqrt{(\cos^2 \delta - \sin^2 \gamma)}, \quad (54)$$

and

$$z_f = r \sin e_f = r \sin \delta. \quad (55)$$

When the equations are combined, the inverse beam pointing equations are

$$\begin{aligned} az_s = & \tan^{-1} [\cos R \cos \mathcal{A} \sqrt{\cos^2 \delta - \sin^2 \gamma} + (\cos R \sin \mathcal{A} \cos \mathcal{B} - \sin R \sin \mathcal{B}) \sin \gamma \\ & + (-\cos R \sin \mathcal{A} \sin \mathcal{B} - \sin R \cos \mathcal{B}) \sin \delta] / [\sin R \sin P \cos \mathcal{A} \\ & - \cos P \sin \mathcal{A}) \sqrt{\cos^2 \delta - \sin^2 \gamma} \\ & + (\sin R \sin P \sin \mathcal{A} \cos \mathcal{B} + \cos R \cos \mathcal{A} \cos \mathcal{B} + \cos R \sin P \sin \mathcal{B}) \sin \gamma \\ & + (-\sin R \sin P \sin \mathcal{A} \sin \mathcal{B} - \cos P \cos \mathcal{A} \sin \mathcal{B} + \cos R \sin P \cos \mathcal{B}) \sin \delta] \quad (56) \end{aligned}$$

$$\begin{aligned} el_s = & \sin^{-1} [(\sin R \cos P \cos \mathcal{A} + \sin R \sin \mathcal{A}) \sqrt{\cos^2 \delta - \sin^2 \gamma} \\ & + (\sin R \cos P \sin \mathcal{A} \cos \mathcal{B} - \sin R \cos \mathcal{A} \cos \mathcal{B} + \sin \mathcal{B} \cos R \cos P) \sin \gamma \\ & + (-\sin R \cos P \sin \mathcal{A} \sin \mathcal{B} + \sin R \cos \mathcal{A} \sin \mathcal{B} + \cos R \cos P \cos \mathcal{B}) \sin \delta]. \quad (57) \end{aligned}$$

Equations (47) and (48) must be computed for each new beam position, and equations (56) and (57) must be computed for each detected target. The error propagation through the equations can be studied by using a truncated Taylor series. The error equations are shown in Appendix B.

So far it was shown that a beam can be pointed toward any point from about $\pm 60^\circ$ in both elevation and azimuth. However the axis of the beam for angle measurement purposes is not necessarily aligned with the horizon. This is called cross level. Nonzero cross-level angles cause two problems. One is that both the azimuth and elevation measurements are subjected to the target's image due to sea-reflected multipath propagation. The other is that if the beam is scanned off in azimuth and elevation, the effects of the cone may limit the elevation angles in which targets may be seen, and the accuracy required of the angle measures in the array may become prohibitive in order to maintain good true azimuth and elevation estimates. Therefore a mechanical cross-level stabilization will be presented.

The drive signal Z for cross level is computed as follows. A unit vector ($x_s = 0$, $y_s = 0$, $z_s = 1$) is taken in stabilized coordinates. The unit vector in the face coordinates is found by using (42), and the x_f and z_f components are

$$x_f = \sin R \cos P \cos \mathcal{A} + \sin P \sin \mathcal{A} \quad (58)$$

and

$$z_f = (-\sin R \cos P \sin \mathcal{B} \sin \mathcal{A} + \sin P \sin \mathcal{B} \cos \mathcal{A} + \cos R \cos P \cos \mathcal{B}). \quad (59)$$

A rotation is performed through cross-level angle Z about the y_f axis until x'_f becomes zero, which is the condition for zero cross level:

$$x'_f = x_f \cos Z + z_f \sin Z = 0 \quad (60)$$

Therefore, from use of (58) through (60), the cross-level angle-drive signal is

$$Z = \tan^{-1} \left[\frac{\sin R \cos P \cos \mathcal{A} + \sin P \sin \mathcal{A}}{-\sin \mathcal{B} (\sin R \cos P \sin \mathcal{A} - \sin P \cos \mathcal{A}) + \cos R \cos P \cos \mathcal{B}} \right]. \quad (61)$$

Since the array is rotated through an angle Z , the face coordinates (x_f, y_f, z_f) must now be rotated through an angle Z to form a new set of face coordinates (x'_f, y'_f, z'_f) :

$$\begin{bmatrix} x'_f \\ y'_f \\ z'_f \end{bmatrix} = S \begin{bmatrix} x_f \\ y_f \\ z_f \end{bmatrix}, \quad (62)$$

where

$$S = \begin{bmatrix} \cos Z & 0 & -\sin Z \\ 0 & 1 & 0 \\ \sin Z & 0 & \cos Z \end{bmatrix}. \quad (63)$$

Therefore the new face coordinates in terms of the stabilized coordinates are

$$\begin{bmatrix} x_s \\ y_s \\ z_s \end{bmatrix} = TWS \begin{bmatrix} x'_f \\ y'_f \\ z'_f \end{bmatrix}, \quad (64)$$

and $(TWS)(TWS)^t = I$. The array drive equations are obtained the same way as before by replacing (x_f, y_f, z_f) with (x'_f, y'_f, z'_f) . These equations are lengthy and therefore are not reproduced here.

STABLE-PLATFORM RADAR ANGLE MEASUREMENTS

For a low-frequency (less than 1 GHz) radar the antenna size is somewhat limited; therefore fairly large beams are anticipated. The question naturally arises as to the accuracy to which angle measurements can be made.

A radar is considered with beamwidths of approximately 5° to 15° . The antenna is assumed to be a phased planer array; therefore four faces will be needed to cover the full 360° in azimuth. It is assumed that the antennas have low sidelobes. It is further assumed that the radar is stabilized in both level and cross level. The azimuth and elevation angles γ and δ are measured at the antenna. Given these measurements, (28) can be used to find the random errors in the true azimuth and elevation. Both γ and δ are necessary, because the beam steers along cones.

The azimuth measurement is first considered. Because the beam is stabilized, there appears to be only a single target in azimuth (target and images are at the same azimuth). Therefore the results quoted earlier from Ref. 3, plotted in Fig. 4, can be used. At a 13-dB S/N the monopulse accuracy is 0.1 beamwidth. The azimuth γ accuracy will be approximately 0.5° or better with no bias error. (This is not the full azimuth error.)

The elevation error is next considered. To cover elevations up to 30° , two receive beams are suggested; one placed $1/2$ beamwidth off the surface and the other up $3/2$ beamwidths. This is shown in Fig. 10. A monopulse channel can be added to the upper beam position, which yields elevation estimates of 0.1 beamwidth at a 13-dB S/N. Therefore from previous results the elevation accuracy would be better than 1.5° . The sea-reflected multipath propagation can be ignored in this region; however in the low-beam position it cannot.

The elevation-measurement technique in the low angle is similar to White's technique [4] described earlier. The upper-beam antenna pattern and the lower-beam antenna pattern are

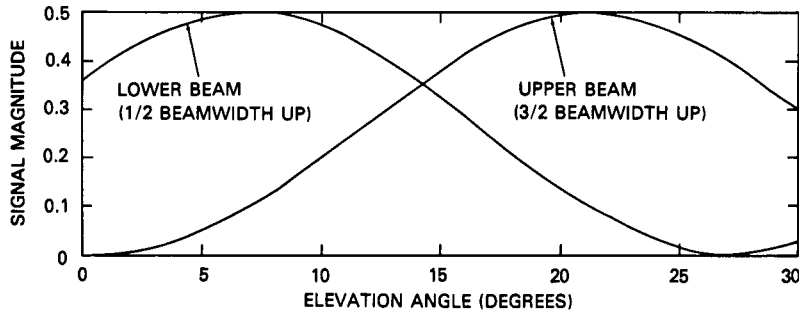


Fig. 10 – Free-space beam patterns in the elevation plane for a broadbeamed radar

subtracted, and the ratio of the resultant to the lower-beam antenna pattern is taken. This ratio is plotted versus elevation angle in Fig 11 for free space and when multipath propagation is present assuming a smooth sea and vertical polarization. First, the figure shows that the sensitivity of the measurement increases as the elevation increases. Second, the multipath has little effect on the measurement except in the vicinity of the first null. The accuracy of the measurement is determined by using the rule of thumb developed earlier (the accuracy of a ratio measurement in noise at a 13-dB S/N is approximately 0.25 times the slope of the error curve). Use of this rule of thumb and the finding of the slopes of the error curve at several locations results in the elevation errors as a function of elevation angle given in Table 3. The elevation estimate becomes better as the elevation angle increases, and the bias error due to multipath propagation can be ignored.

The true azimuth error can then be found using curves such as in Fig. 8. For a 13-dB S/N it appears that by combining the error due to the cone effect with the azimuth measurements the total azimuth error can be held to less than 1° with essentially no bias error. For stronger S/N the results improve. For example at 23 dB the results would improve about three-fold. In summary it appears that the planer phased array can make adequate angle measurements if the array is cross-level stabilized.

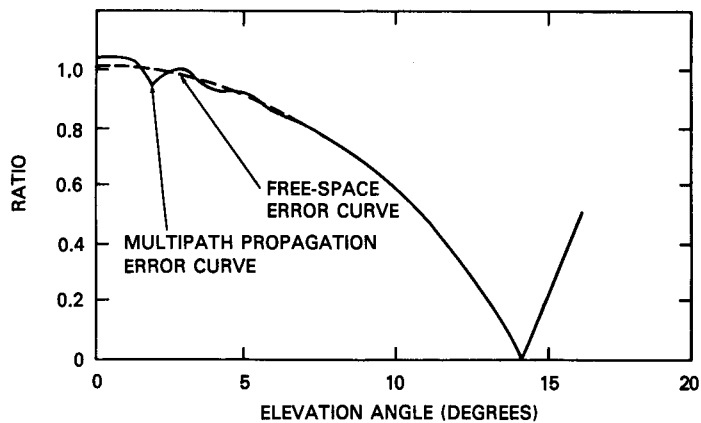


Fig. 11 – Ratio of the difference in signal level in Fig. 10 to the signal level of the lower beam (free-space error curve) and, compared to that, the same ratio for smooth-sea multipath conditions

Table 3 — Elevation Error as a Function of Elevation Angle for a 13-dB S/N

Elevation (deg)	Slope	Elevation Error (deg)
0	0	?
4	24	6
8	18	4.5
12	8	2

UNSTABLE-PLATFORM RADAR ANGLE MEASUREMENTS

In the previous section the radar was assumed to be mechanically cross-level stabilized and electronically stabilized in level. Under that assumption the steered azimuth could be measured accurately, because the target and image appear as a point target in that plane. The elevation was estimated so as to find the true azimuth, which is coupled to the elevation by the beam steering along conical sections. The problem that will now be investigated is the presence of cross level, causing the target and image to appear at different locations in both the steered azimuth and elevation. This is illustrated in Fig. 12.

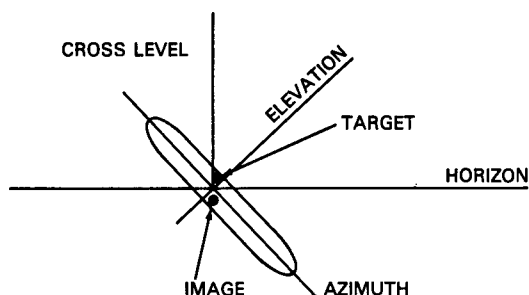


Fig. 12 — Fan beam tilted in cross level

We begin by considering a simple case. Let the array be normal to the ship and pointed toward the bow of the ship ($\mathcal{A} = 0, \mathcal{B} = 0$) and let the pointing angle be ($az_s = 0, el_s = 0$). Let the pitch P be zero and the roll R be finite. From (47) and (48) the peak of the beam in the face coordinates comes at ($\gamma = 0, \delta = 0$) and the beam is tilted in cross level by the roll R of the ship given by (61). If the target is somewhere in the beam at angles az_s and el_s , then the azimuth and elevation angles in the array coordinates are

$$\gamma_T = \sin^{-1}(\cos R \cos el_s \sin az_s + \sin R \sin el_s) \quad (65)$$

and

$$\delta_T = \sin^{-1}(-\sin R \cos el_s \sin az_s + \cos R \sin el_s). \quad (66)$$

The image is located at az_s and $-el_s$; thus its azimuth and elevation in the array coordinates are

$$\gamma_I = \sin^{-1}(\cos R \cos el_s \sin az_s - \sin R \sin el_s) \quad (67)$$

and

$$\delta_I = \sin^{-1} (-\sin R \cos \text{el}_s \sin \text{az}_s - \cos R \sin \text{el}_s). \quad (68)$$

In general the azimuth and elevation in the array coordinates are different for both the target and image. This causes problems in measuring the angles. The signal returns assuming geometrical optics are

$$S_{\Sigma} = A [G_{\gamma} (\gamma_T) G_{\delta} (\delta_T) e^{+j\theta} + \rho G_{\gamma} (\gamma_I) G_{\delta} (\delta_I) e^{+j\theta + \phi}], \quad (69)$$

$$S_{\gamma\Delta} = A [H_{\gamma} (\gamma_T) G_{\delta} (\delta_T) e^{+j\theta} + \rho H_{\gamma} (\gamma_I) G_{\delta} (\delta_I) e^{+j\theta + \phi}] \quad (70)$$

and

$$S_{\delta\Delta} = A [G_{\gamma} (\gamma_T) H_{\delta} (\delta_T) e^{+j\theta} + \rho G_{\gamma} (\gamma_I) H_{\delta} (\delta_I) e^{+j\theta + \phi}]. \quad (71)$$

where G_{γ} and G_{δ} are sum patterns in azimuth and elevation, H_{γ} and H_{δ} are difference patterns in azimuth and elevation, S_{Σ} is a sum signal, $S_{\gamma\Delta}$ and $S_{\delta\Delta}$ are difference signals in azimuth and elevation, and $\theta = (2\pi h/\lambda) \sin \text{el}$ is the relative phase shift between the target and the image.

Equations (65) through (68) could be substituted into (69) through (71). The unknowns are the signal amplitude A , azimuth az_s , elevation el_s , reflection coefficient ρ , and phase shift at the sea surface ϕ . Thus this model has five unknowns. Using the sum signal (69) as a phase reference, the magnitude and phase can be found in (70) and (71). Therefore there are five equations. However the solution could be quite difficult because of the nonlinearity of these equations. One solution technique is to use a least-square solution formulated as follows. Given a set of functional relations

$$S_i = f(X_1, X_2, X_3, \dots, X_N), \quad i = 1, 2, \dots, N, \quad (72)$$

if the S_i are measured, denoted as S_i^M , then the following relation holds:

$$\sum_{i=1}^N [S_i^M - f(X_1, X_2, \dots, X_N)]^2 = 0. \quad (73)$$

The values of X_i can be estimated by using a search technique which minimizes (73). For complex problems this search can be time consuming and may be ill conditioned in regions. In addition many locally good solutions may not be correct. The nature of the search for given problems must be investigated in great detail. This technique is basically the same as the one described in Ref. 6.

The solution for the true azimuth and elevation as formulated assumes an image located at the same azimuth as the target and with the opposite elevation angle. If the scattering surface does not operate in this manner, more equations can be used by changing the beam pointing angles or beam shapes to obtain these additional equations, and the model must be made more complex with more unknowns.

A technique for obtaining the azimuth when multipath propagation and cross level is present was suggested by Bernard Lewis, and a simple tentative solution was worked out by Lewis and the present author as described below. The glint appears in only the elevation plane even though the beam is not cross leveled, and the target measured angle will be somewhere along the line connecting the target and image as shown in Fig. 13. The apparent target azimuth position in the unrotated frame of reference (az, el) is

$$\text{az} = c + d. \quad (74)$$

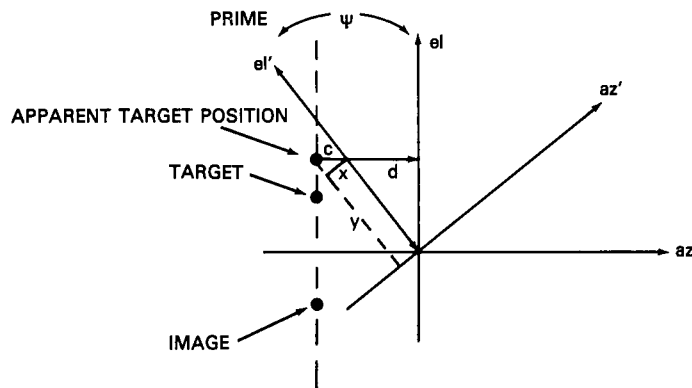


Fig. 13 — Geometry for obtaining the azimuth when multipath propagation and antenna cross level are present

However what is measured is x and y in the rotated reference frame (az' , el'). The values of c and d can be related to x and y by

$$c = x \cos \psi \tag{75}$$

and

$$d = y \sin \psi; \tag{76}$$

therefore the azimuth is

$$az = x \cos \psi + y \sin \psi. \tag{77}$$

The azimuth can be found because the apparent target position lies on the line connecting the target and image. Work is continuing on this concept.

SUMMARY

The intent of this report is to consider angle-measurement accuracies for a broadbeam search radars whose antenna is a planer array. Two basic systems were considered: an antenna stabilized against ship motion and an unstabilized antenna system.

The stabilized antenna by normal monopulse techniques yields good steered azimuth estimates, which must be converted to true azimuth by using the target elevation. A means of estimating elevation with no bias errors was given which was poor near the horizon and improved to that achievable by a monopulse measurement at about 3/4 beamwidth above the horizon. These estimates are good enough to adequately correct the steered azimuth to the true azimuth with an accuracy of less than 1° for minimal detectable signals ($S/N = 13$ dB). The mechanical stabilization in cross level and electronic stabilization in level have other advantages as well. First, vertical polarization is postulated, which improves the detections when multipath propagation is present at the low angles. Vertical polarization can be maintained with cross-level errors but at the expense of a complex feed and dipole structure on the array. Also, the beams can be accurately pointed in level to minimize the multipath effects and maintain power in the desired directions. Finally, if the array is tilted in cross level, the ability to scan to high elevation angles off broadside becomes nonexistent, and better and better steered elevation estimates must be made to provide adequate estimates of true azimuth. Other alternatives

to a mechanical stabilization in cross level and full-phased array is a full mechanical stabilization. The antenna need then only be column fed to achieve azimuth steering. Of course multiple receive beams are required in elevation. However the difficulty with either approach is that mechanical movement of a large antenna is required. In this author's best opinion, when the antenna is cross-level stabilized, adequate azimuth measurements can be made.

The second method considered was no mechanical stabilization but steering in azimuth and elevation electronically. The beam is level stabilized but not cross leveled. A means of obtaining an estimate of the target's azimuth and elevation was formulated by assuming the target and image were at the same azimuth and symmetrically located above and below the water. A solution technique involving least squares was suggested for obtaining a solution. However no results are yet available. The difficulties with this method are that the solution is complex, the polarization changes as the cross level moves, and very accurate elevation estimates are required for large cross-level angles and large scan angles. However no mechanical stabilization is required. Furthermore the method is only suggested and has not been verified.

The concept proposed by Lewis (last paragraph of the preceding section) would provide good estimation of azimuth when the antenna is not cross-leveled and sea-reflected multipath propagation is present.

REFERENCES

1. M.I. Skolnik, editor, *Radar Handbook*, McGraw-Hill, 1970.
2. L.V. Blake, "Machine Plotting of Radio/Radar Vertical-Plane Coverage Diagrams," NRL Report 7098, June 25, 1970.
3. D.K. Barton, *Radar System Analysis*, Prentice-Hall, 1964.
4. W.D. White, "Low-Angle Radar Tracking in the Presence of Multipath," IEEE Trans. on Aerospace and Electronic Systems **AES-10** (No. 6), 835-852 (Nov. 1974).
5. S.K. Meads, "A Fixed-Array, High-Data-Rate Search and Height-Finding Radar," NRL Report 5905, May 14, 1963.
6. P.Z. Peebles, Jr., "Multipath Angle Error Reduction Using Multiple-Target Methods," IEEE Trans. on Aerospace and Electronic Systems **AES-7** (No. 6), 1123-1130 (Nov. 1971).

Appendix A COMPLEX MODELS

The simple geometrical solutions in the main text are valid only when the sea is smooth. In this appendix we consider when these solutions are not valid.

The multipath reflection is first considered. Consider forward scattering from a mirror surface as shown in Fig. A1. The classical physical optics solution would show a large first Fresnel zone and succeeding zones alternating in phase and all in the shape of an ellipse [A1, A2]. The forward scatter is strong when the angle of incidence is equal to the angle of reflection. The size of the zones can be fairly large for low grazing angles. For example at a radar of wavelength 10 cm and a grazing angle of 0.59° , the semimajor and semiminor axis of the first ellipse is 615 by 6.6 meters [A2]. When the source is a point source, most of the contributions are usually considered in the first zone, and the remaining zones more or less cancel out. However if the beam is narrow and illuminates small areas of the Fresnel zones, the forward scattering changes, because the contributions from the various regions are weighted differently than when a point source is considered. For targets at low elevation angles the first Fresnel zones appear at a fairly large distance from the radar, and with normal beamwidths on 2D radars the illumination of the most important Fresnel zones can be considered as though they were illuminated by point source. However at high elevation angles the first Fresnel zone moves in toward the source and the beam weight may have to be taken into account. A constant-power contour of two tilted beams on the mirror is shown in Fig. A2. We assume that the peculiar strong contributions lie in a small region near the intersection of the contours, although there may be some geometries where this is not true.

For rough surfaces the forward scattering is much more complicated. Two experiments will be considered. In Ref. A1 an experiment is described in which the direct path and reflected path over a rough sea was separated by using narrow-beam antennas. The illumination was provided by a broad-beam pulsed radar with a 9-cm wavelength. The experimental results are shown in Fig. A3. The results show a constant signal voltage on the direct wave because of the absence of multipath propagation. The indirect (reflected signal) shows an interference effect by bouncing up and down with a time constant of a 0.5 s.

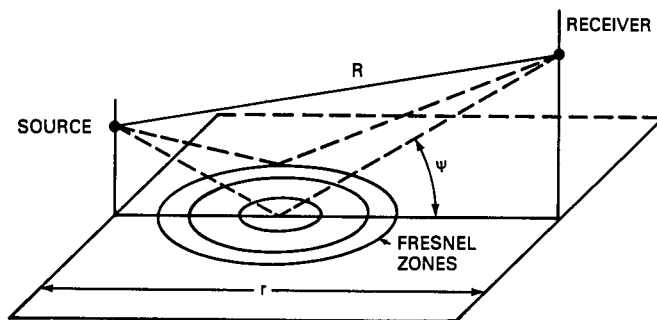


Fig. A1 – Geometry of forward scatter from a mirror

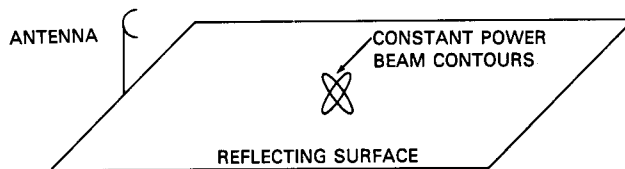


Fig. A2 – Constant-beam contours on a reflecting surface for two oppositely tilted fan beams

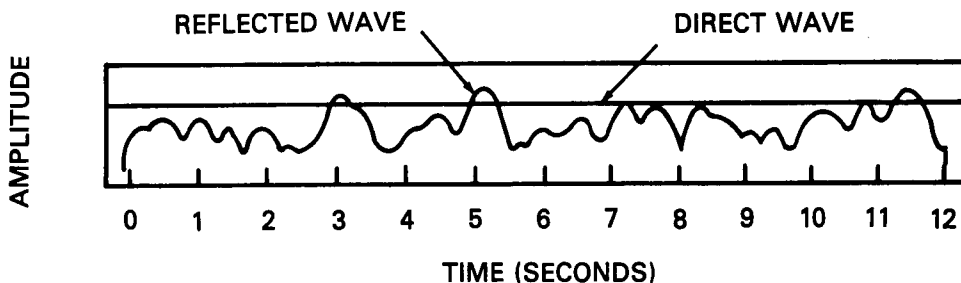


Fig. A3 – Variation with time of 9-cm horizontally polarized radiation reflected from a rough sea at a grazing angle of 11° (from Ref. A1)

In Ref. [A2] another experiment is described, which was conducted by Ford and Oliver. The experiment used a narrow beam to examine the scattering from various reflecting areas. The results basically show that there is a large region of low-level diffuse scatter extending over a large region away from the more-or-less specular Fresnel zone.

Thus for the forward scatter we ignore the beam shape and the diffuse scatter. Therefore the geometrical optics solution with ρ being variable is valid. However there may be situations where these assumptions break down.

Next the target model is considered. If a target reradiates energy at about the same magnitude along the direct and indirect paths and does not change with time, it is considered a point target. For height determination it really does not matter (as long as there is signal strength) if the reradiation is different along the direct or indirect paths.

In summary, many factors affect the height determination in radars. Some of them are the surface-reflection effects, target characteristics, and signal strength across the antenna aperture. Others are propagation effects such as refraction and ducting. Most of these effects are not considered in the analysis.

REFERENCES

- A1. D.E. Kerr, et al., editor, *Propagation of Short Radar Waves*, Vol. 13, Radiation Laboratory Series, MIT, McGraw-Hill, 1951.
- A2. P. Beckman and A. Spizzichino, *The Scattering of Electromagnetic Waves from Rough Surfaces*, Pergamon Press, 1963.

Appendix B
ERROR PROPAGATION THROUGH TRANSFORMATIONS

The error propagation from the array measurements to the stabilized-coordinate equations, (56) and (57), are studied by a truncated Taylor series expansion. The series can be written as

$$\begin{bmatrix} az_s \\ el_s \end{bmatrix} = \begin{bmatrix} az_s^0 \\ el_s^0 \end{bmatrix} + \begin{bmatrix} \frac{\partial az_s}{\partial \gamma} & \frac{\partial az_s}{\partial \delta} \\ \frac{\partial el_s}{\partial \gamma} & \frac{\partial el_s}{\partial \delta} \end{bmatrix} \begin{bmatrix} \Delta\gamma \\ \Delta\delta \end{bmatrix}. \quad (B1)$$

with the definition

$$C = \begin{bmatrix} \frac{\partial az_s}{\partial \gamma} & \frac{\partial az_s}{\partial \delta} \\ \frac{\partial el_s}{\partial \gamma} & \frac{\partial el_s}{\partial \delta} \end{bmatrix} \quad (B2)$$

the errors are

$$cov \begin{bmatrix} az_s \\ el_s \end{bmatrix} = C \left[cov \begin{bmatrix} \gamma \\ \delta \end{bmatrix} \right] C^T. \quad (B3)$$

The elements of C are

$$\begin{aligned} \frac{\partial az_s}{\partial \alpha} &= \cos az_s [\cos R \cos \mathcal{A} (-\sin \gamma \cos \gamma) / \sqrt{\cos^2 \delta - \sin^2 \gamma} + (\cos R \sin \mathcal{A} \cos \mathcal{B} \\ &\quad - \sin R \sin \mathcal{B}) \cos \gamma] \\ &\quad - \sin az_s [(\sin R \sin P \cos \mathcal{A} - \cos P \sin \mathcal{A}) (-\cos \gamma \sin \gamma) / \sqrt{\cos^2 \delta - \sin^2 \gamma} \\ &\quad + (\sin R \sin P \sin \mathcal{A} \cos \mathcal{B} + \cos P \cos \mathcal{A} \cos \mathcal{B} + \cos R \sin P \sin \mathcal{B}) \cos \gamma], \quad (B4) \end{aligned}$$

$$\begin{aligned} \frac{\partial az_s}{\partial \delta} &= \cos az_s \left[\frac{\cos R \cos \mathcal{A} (-\cos \delta \sin \delta)}{\sqrt{\cos^2 \delta - \sin^2 \gamma}} \right. \\ &\quad \left. + (-\sin \mathcal{A} \sin \mathcal{B} \cos R - \sin R \cos \mathcal{B}) \cos \delta \right] \\ &\quad - \sin az_s [(\sin R \sin P \cos \mathcal{A} - \cos P \sin \mathcal{A}) \\ &\quad + (-\cos \delta \sin \delta / \sqrt{\cos^2 \delta - \sin^2 \gamma}) \\ &\quad + (-\sin R \sin P \sin \mathcal{A} \sin \mathcal{B} - \cos P \cos \mathcal{A} \sin \mathcal{B} + \cos R \sin P \cos \mathcal{B}) \cos \delta], \quad (B5) \end{aligned}$$

$$\begin{aligned} \frac{\partial el_s}{\partial \gamma} &= \frac{1}{\cos el_s} [(\sin R \cos P \cos \mathcal{A} + \sin P \sin \mathcal{A}) (-\sin \gamma \cos \gamma / \sqrt{\cos^2 \delta - \sin^2 \gamma}) \\ &\quad + (\sin R \cos P \sin \mathcal{A} \cos \mathcal{B} - \sin P \cos \mathcal{A} \cos \mathcal{B} + \cos R \cos P \sin \mathcal{B}) \cos \gamma] \quad (B6) \end{aligned}$$

and

$$\begin{aligned} \frac{\partial e_{l_s}}{\partial \delta} &= \frac{1}{\cos e_{l_s}} [(\sin R \cos P \cos \mathcal{A} + \sin P \sin \mathcal{A}) \\ &\quad (-\cos \delta \sin \delta / \sqrt{\cos^2 \delta - \sin^2 \gamma}) \\ &\quad + (-\sin R \cos P \sin \mathcal{A} \sin \mathcal{B} + \sin P \cos \mathcal{A} \sin \mathcal{B} + \cos R \cos P \cos \mathcal{B}) \cos \delta]. \quad (\text{B7}) \end{aligned}$$